

# An improved Monte Carlo study of coherent scattering effects of low energy charged particle transport in Percus-Yevick liquids

W. J. Tattersall,<sup>1,2</sup> D. G. Cocks,<sup>2</sup> G. J. Boyle,<sup>2</sup> and R. D. White<sup>2</sup>

<sup>1</sup>*Research School of Physics and Engineering,  
The Australian National University, Canberra, ACT 0200, Australia*

<sup>2</sup>*College of Science, Technology and Engineering,  
James Cook University, Townsville 4810, Australia*

## Abstract

We generalize a simple Monte Carlo (MC) model for dilute gases to consider the transport behavior of positrons and electrons in Percus-Yevick model liquids under highly non-equilibrium conditions, accounting rigorously for coherent scattering processes. The procedure extends an existing technique [Wojcik and Tachiya, Chem. Phys. Lett. **363**, 3–4 (1992)], using the static structure factor to account for the altered anisotropy of coherent scattering in structured material. We identify the effects of the approximation used in the original method, and develop a modified method that does not require that approximation. We also present an enhanced MC technique that has been designed to improve the accuracy and flexibility of simulations in spatially-varying electric fields. All of the results are found to be in excellent agreement with an independent multi-term Boltzmann equation solution, providing benchmarks for future transport models in liquids and structured systems.

## I. INTRODUCTION

The precise behavior of electrons and positrons traveling through matter is of vital importance in many new and established technologies. Applications such as solar cells [2], radiation dosimetry [3], material pore-size classification [4] and positron emission tomography [5] all require an understanding of the fundamental physical processes involved, including accurate knowledge of energy deposition, macroscopic behaviors, and loss rates.

Although the behavior of high-energy particles can be simulated quite accurately with condensed history techniques [6], at low energies it is important to model the individual interactions of particles colliding with the background material, and thereby monitor discrete energy losses and processes that change the number of particles in the system. In the systems that we are investigating, the number density of the charged particles is low enough that the Debye wavelength greatly exceeds the dimensions of the the system, which is known as the “swarm” limit of an ionized gas [7].

One successful approach to modeling such systems is by solving the Boltzmann equation [8], which is an equation of continuity in phase space. Often this approach is limited to idealized geometries, due to complexities in the numerical solution and application of boundary conditions. However, many real-world systems are too complex for such an approach to be effective, and in any case, alternative methods should ideally be used for verification.

The pre-eminent alternative is to use Monte Carlo simulations, which have been widely employed for such purposes [9–13] ever since computers have been powerful enough to implement them [14]. Monte Carlo simulations are very flexible, and can easily include features from systems that are quite difficult to model in any other manner, such as interfacial effects, secondary particles, and inhomogenous media.

Accurate simulations of condensed systems must include the effects of coherent scattering, where the incoming electrons and positrons interact with many particles of the system at once. This can occur when the de Broglie wavelength of the low energy electrons and positrons is longer than the mean distance between molecules of the condensed matter [15]. It is common to ignore these effects in Monte Carlo simulations of liquids [16], because they are usually insignificant for electrons and positrons with energies of greater than  $\sim 10 - 20$  eV. However, to accurately treat particle transport at low energies, we must include these collective effects, usually by way of the medium’s dynamic structure factor  $S(\Delta\mathbf{k}, \Delta\omega)$  [15],

which contains information about the medium’s characteristic allowed transfers of momentum  $\hbar\Delta\mathbf{k}$  and energy  $\hbar\omega$ . The dynamic structure is exactly what is measured by coherent neutron scattering experiments such as [17].

The present study will describe a new Monte Carlo implementation that models structured matter using a static structure factor,  $S(\Delta\mathbf{k})$ , which is an integrated form of the dynamic structure factor. We first use a technique described by Wojcik and Tachiya [1] to incorporate the static structure factor into our Monte Carlo model, but we assert that this method is only accurate for a certain subset of cases. We subsequently extend this technique to overcome its limitations. The Percus-Yevick static structure factor is a simple analytic static structure factor [18] that can be used as a benchmark to verify the accuracy of our simulation. We have performed simulations of a number of Percus-Yevick systems at a range of reduced electric field strengths, and we compare our results with those obtained by solving the Boltzmann equation detailed in [8].

We begin this study with a discussion of the Boltzmann equation approach to coherent scattering. We follow this with a brief description of typical Monte Carlo collision mechanics for elastic processes in section II A. We then use the Boltzmann equation coherent scattering rates to derive a set of modified cross sections in section II B, and identify the approximation made in Wojcik and Tachiya’s original method [1]. In section II C, we describe a new method that we have developed for performing simulations in spatially-varying electric fields. The model system that we are studying is extensively described in section III, and finally, we present our results in section IV, including comparisons with the results from both our implementation of Wojcik and Tachiya’s method, as well as an independent Boltzmann equation solution.

## II. THEORY

### A. Coherent scattering

Designing simulations of swarm transport in liquids and dense gases presents additional challenges compared to the ideal gas case. Because the inter-particle spacing of the neutral particles is often less than the de Broglie wavelength of the swarm particles, the swarm particles must often interact with several neutral particles at the same time, which means that

any spatial or temporal correlations between said particles will have an effect on scattering events. The Cohen-Lekner theory of electron transport [19] describes these effects in terms of two rates of transfer – momentum and energy – that occur independently.

Cohen and Lekner express the electron distribution function in a basis of spherical harmonics. They then modify the standard Boltzmann collision integral to include the dynamic structure factor  $S(\Delta\mathbf{k},\omega)$ , as motivated by van Hove’s definition of the ensemble cross section [20], and then show that when the necessary integrals have been performed, the dependence is only upon the static structure factor.

Upon solving the equations for the time evolution of the distribution function, they ascribe a physical meaning to two of the mean free path lengths that appear in the collision integral expansion. The first fully determines the rate of energy transferred from the swarm particles. It is independent of the structure of the medium, and is given by the mean free path corresponding to single-particle elastic scattering:

$$\Lambda_0 = (n_0\sigma_m)^{-1} = \left( n_0 2\pi \int_0^\pi d\chi \sin\chi (1 - \cos\chi) \sigma_{sp}(\epsilon, \chi) \right)^{-1}, \quad (1)$$

where  $n_0$  is the number density of the neutral molecules,  $\sigma_{sp}(\epsilon, \chi)$  is the angle-differential elastic cross section for scattering with a single particle (also known as the binary or gas-phase cross section), and  $\sigma_m$  is the usual definition of the momentum transfer cross section in the absence of coherent effects. Throughout the present work,  $\epsilon$  refers to the relative energy in the centre-of-mass frame during a collision, and  $\chi$  represents the angle through which the relative velocity is changed.

The second mean free path partly includes the effect of the medium and contains all information about the rate at which momentum is transferred:

$$\Lambda_1 = (n_0\tilde{\sigma}_m)^{-1} = \left( n_0 2\pi \int_0^\pi d\chi \sin\chi (1 - \cos\chi) \sigma_{sp}(\epsilon, \chi) S(\Delta\mathbf{k}) \right)^{-1}, \quad (2)$$

where  $S(\Delta\mathbf{k})$  is the static structure factor as a function of the momentum transferred and  $\tilde{\sigma}_m$  represents a structure modification of the momentum transfer cross section.

In a recent paper [21], the explicit rates of energy and momentum transfer were calculated with the inclusion of structure in the Boltzmann equation. The components of this transfer

due to the collision term, in the case of zero temperature, are:

$$\begin{aligned} \left. \frac{d}{dt} \langle n m \mathbf{v} \rangle \right|_{\text{coll}} &= -\langle n_0 v \tilde{\sigma}_m(v) m \mathbf{v} \rangle + O(\omega) + O\left(\frac{m}{m_0}\right) \\ &= -\langle v \Lambda_1^{-1}(v) m \mathbf{v} \rangle \end{aligned} \quad (3)$$

and

$$\begin{aligned} \left. \frac{d}{dt} \langle n \epsilon \rangle \right|_{\text{coll}} &= -2 \frac{m}{m_0} \langle n_0 v \sigma_m(v) \epsilon \rangle + O(\omega^2) + O\left(\left(\frac{m}{m_0}\right)^2\right) \\ &= -2 \frac{m}{m_0} \langle v \Lambda_0^{-1}(v) \epsilon \rangle, \end{aligned} \quad (4)$$

where  $\langle \rangle$  represents averaging over velocity space and  $n$  is the number density of the charged particles.

Note that these representative mean free paths should be considered independently, and should be only thought of as an average rate of transfer of the relevant quantity, rather than as a prescription for separate collision events. We define the ratio  $\Gamma(\epsilon) \equiv \Lambda_0/\Lambda_1 = \tilde{\sigma}_m/\sigma_m$ . In the dilute gas case,  $\Gamma(\epsilon) = 1$ , because the static structure factor of a dilute gas is unity for all momentum transfers. However, in a structured medium such as a dense gas or a liquid, the ratio can deviate markedly from unity. If  $\Gamma(\epsilon) < 1$ , there is noticeably less momentum transfer than in the single-particle scattering case, which can be interpreted as a preference towards forward scattering events. In the opposite case of  $\Gamma(\epsilon) > 1$ , more momentum transfer occurs, which causes the particle to change direction without losing as much energy as it would in the single-particle scattering.

In the case of an isotropic single-particle elastic cross section,  $\sigma_{sp}(\epsilon, \chi) = \frac{1}{4\pi} \sigma_{sp}(\epsilon)$ , as in the model described in section III, and the ratio  $\Gamma(\epsilon)$  reduces to:

$$\Gamma(\epsilon) = \frac{\Lambda_0}{\Lambda_1} = \frac{1}{2} \int_0^\pi d\chi \sin \chi (1 - \cos \chi) S\left(\frac{2(2m\epsilon)^{1/2}}{\hbar} \sin\left(\frac{\chi}{2}\right)\right), \quad (5)$$

where we have assumed the static structure factor depends only on the magnitude of  $\Delta \mathbf{k}$ , and  $|\hbar \Delta \mathbf{k}| = \hbar \Delta k \approx 2\sqrt{2m\epsilon} \sin \frac{\chi}{2}$  in the limit of a small mass ratio  $m/m_0$ . Throughout the present work,  $m$  refers to the mass of each charged particle, and  $m_0$  the mass of each neutral molecule. This form of  $\Gamma(\epsilon)$  is sometimes called the angle-integrated static structure factor,  $\bar{S}(\epsilon)$ , and it is this form of the structure factor that is used in several previous works [1, 8].

In the case of dilute gases, where  $S(\Delta \mathbf{k}) = 1$ , the energy and momentum transfer rates converge, yielding the single-scattering model in which every energy transfer is accompanied

by a momentum transfer. When the transfer rates differ, however, this theory is not directly applicable to Monte Carlo modeling because it does not give a microscopic description of how much energy and momentum is transferred in each collision between swarm particles and neutral particles.

## B. Sampling coherent scattering in Monte Carlo simulations

Our Monte Carlo simulations are built around sampling sets of scattering cross sections,  $\sigma$ , that define the probabilities of all interactions between the charged particles and the medium. Each cross section represents a single type of scattering process, for example elastic, direct ionization, or a particular electronic excitation of the neutral. They usually depend upon the relative speed of the charged particle during a collision, and on the scattering angle  $\chi$ . In the case of a cold background medium, the collision frequency is simply given by:

$$\nu = n_0 v \sigma_{tot}(v), \quad (6)$$

where  $v$  is the speed of the charged particle and  $\sigma_{tot}(v)$  is the integrated sum of all differential cross sections at that speed [22]. This quantity is used to stochastically sample the time between each collision (further described in section II C). When a collision is simulated, a specific cross section is randomly selected according to the relative probabilities of the available cross sections [23]. In the case of single-scattering collisions with independent gas molecules, the amount of energy and momentum transferred is fully determined by the initial energy and the scattering angles.

For structured materials, an approximate theory has been developed by Wojcik and Tachiya [1], who propose a mechanistic model of electron transport in rare gas liquids. In what follows, we have extended this model to be more generally applicable to other systems, highlighting the approximations and associated errors of Wojcik and Tachiya's model.

The presence of structure requires the introduction of additional microscopic processes that, at a macroscopic level, produce the same rate of energy and of momentum transfer as in the Boltzmann equation formalism detailed in section II A. We choose to do this by separating the original, single-particle elastic cross section into three different processes depending on the ratio  $\Gamma(\epsilon)$ , as illustrated in Fig. 2. These processes have cross sections, labeled by which quantities are affected in the collision:  $\sigma_{\text{both}}$ ,  $\sigma_{\text{momentum}}$  and  $\sigma_{\text{energy}}$ . The

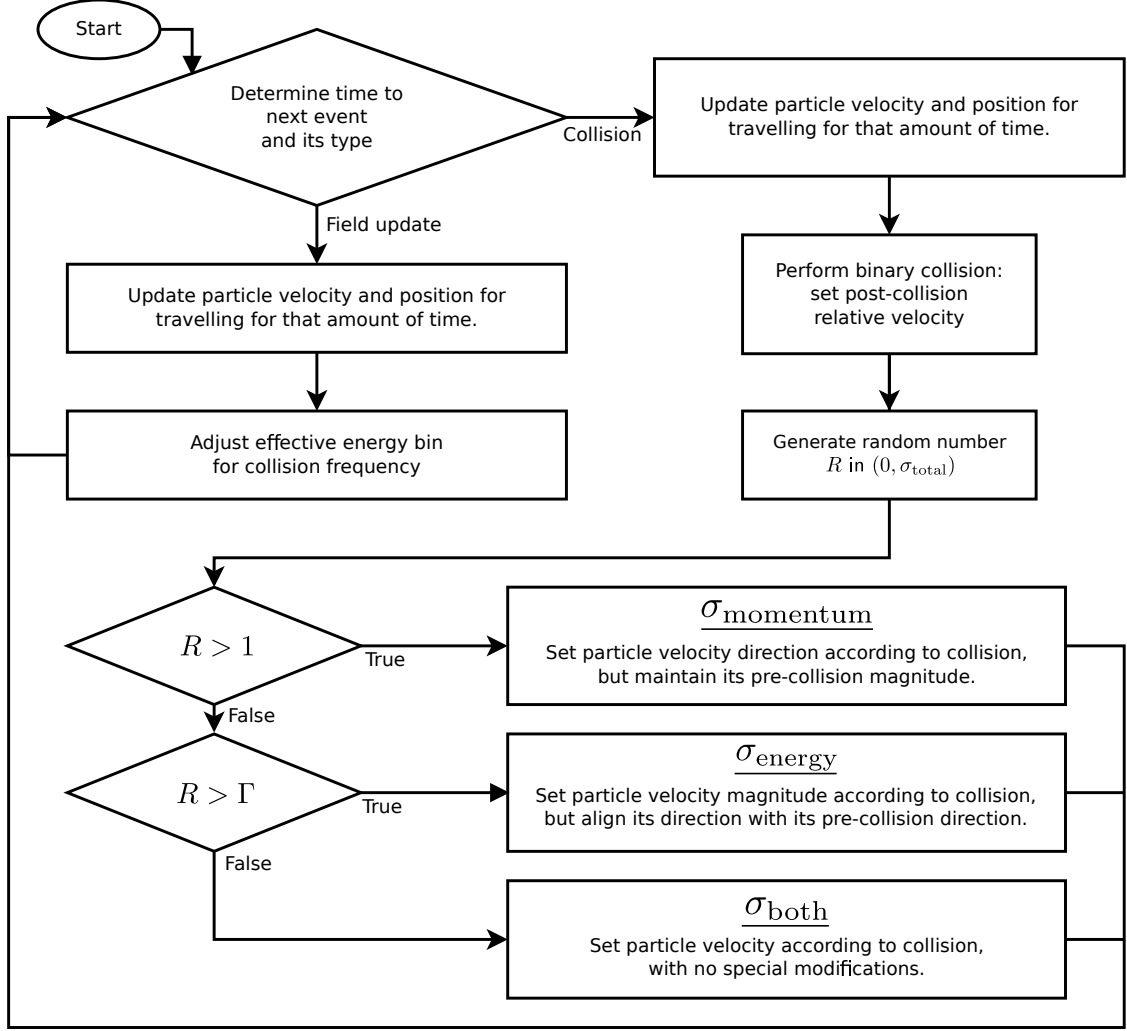


Figure 1. Flowchart detailing how electric fields and coherent scattering are implemented in the SSMC code.

result of a collision from process  $\sigma_{\text{both}}$  is identical to that of a regular single-particle scattering collision. For  $\sigma_{\text{energy}}$ , we start with a regular single-particle scattering collision, but set the post-collision direction of motion for the particle to be unchanged. This has the effect of transferring a minimal amount of momentum whilst maintaining the same energy transfer as in  $\sigma_{\text{both}}$ . For  $\sigma_{\text{momentum}}$ , we perform a regular single-particle scattering collision, but scale the post-collision particle speed to be equal to that before the collision. This results in exactly zero transfer of energy, but some change of vector momentum.

The path lengths  $\Lambda_0$  and  $\Lambda_1$  in section II A correspond to transfer rates of  $\nu_m = vn_0\sigma_m = v/\Lambda_0$  and  $\tilde{\nu}_m = vn_0\tilde{\sigma}_m = v/\Lambda_1$  for energy and momentum respectively, where  $v$  is the speed of the charged particle. To achieve these rates, we combine the cross sections in various

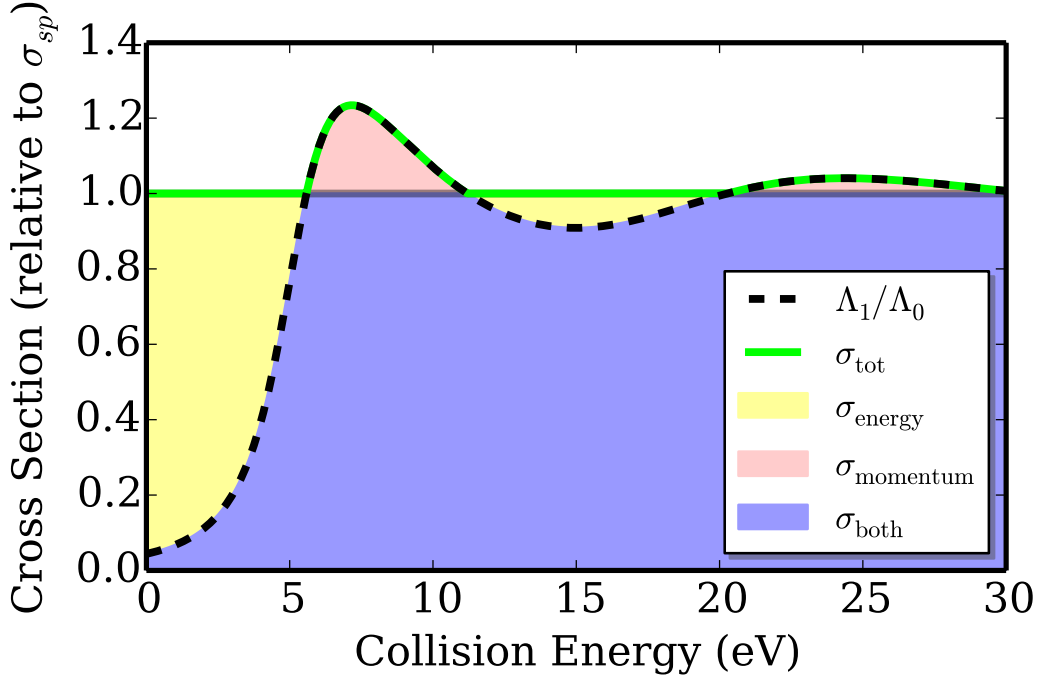


Figure 2. Schematic diagram of the various elastic cross-sections used in simulating a Percus-Yevick liquid ( $\phi = 0.4$ ). All quantities are given relative to the elastic cross-section for a single particle. Note that the  $\sigma_{\text{tot}} \geq \sigma_{\text{sp}}$ .

ratios depending on the value of  $\Gamma(\epsilon) = \Lambda_0/\Lambda_1$ . If  $\Gamma(\epsilon) < 1$  we wish to decrease the rate of momentum transfer, while maintaining energy transfer, and so choose  $\sigma_{\text{both}}^{\Gamma < 1} = \Gamma(\epsilon)\sigma_{\text{sp}}$ ,  $\sigma_{\text{energy}}^{\Gamma < 1} = (1 - \Gamma(\epsilon))\sigma_{\text{sp}}$  and  $\sigma_{\text{momentum}}^{\Gamma < 1} = 0$ . In the opposite case,  $\Gamma(\epsilon) > 1$ , we achieve an increased rate of momentum transfer, by setting  $\sigma_{\text{both}}^{\Gamma > 1} = \sigma_{\text{sp}}$ ,  $\sigma_{\text{momentum}}^{\Gamma > 1} = (\Gamma(\epsilon) - 1)\sigma_{\text{sp}}$  and  $\sigma_{\text{energy}}^{\Gamma > 1} = 0$ . This gives a total elastic cross section of  $\sigma_{\text{tot}} = \max(1, \Gamma(\epsilon))\sigma_{\text{sp}}$ . The complete Monte Carlo procedure, which we refer to as the “Static Structure Monte Carlo” (SSMC) method, is shown as a flowchart in Fig. 1.

The procedure outlined above is designed to reproduce the rates of energy and momentum transfer in equations (1) and (2). However, it is not obvious that our construction of the microscopic processes achieves this goal. In Appendix A, we show that such a sampling process involving these cross sections does indeed satisfy these requirements, to within the order of the mass ratio  $m/m_0$  as mentioned earlier. These differences are small enough that they are unlikely to effect electron-atom simulations, though they may be significant in systems where ions serve as the charged particles.

Wojcik and Tachiya [1] studied liquid argon according to the method described above, but their mechanistic model, hereafter referred to as the WT method, effectively capped the value of  $\Gamma(\epsilon)$  such that it never exceeded unity. This meant that their total collision frequency was unaltered from the single-particle scattering case, and simulation of the particles in the energy regions where  $\Gamma(\epsilon)$  exceeded 1 could only be considered approximately accurate. The difference between the SSMC and WT methods [1] is shown in Fig. 2, where the regions labeled  $\sigma_{\text{momentum}}$  are absent in their model, and the total cross section modified accordingly, so that it is simply  $\sigma_{sp}$ . For the aforementioned study of liquid argon, such modifications were only required in a small energy range for the structure factor that they employed. One of the purposes of the present study is to determine how this approximation affects the results for a benchmark Percus-Yevick model, where the approximation is more significant.

### C. Precise treatment of electric fields in Monte Carlo simulations

Electric fields present a particular challenge for this style of Monte Carlo simulation. As the collision frequency  $\nu$  of a given charged particle is dependent on its energy  $\epsilon$  (see equation 6), the time between collisions  $\tau$  can be altered by the change of energy of the particle due to the electric field, even as it is undergoing the transport between collisions. Mathematically, the probability of a time between collisions greater than  $\tau$  can be expressed as [14]

$$P(\tau) = \exp\left(-\int_0^\tau \nu(\epsilon(t)) dt\right), \quad (7)$$

where the charged particle's energy is time dependent due to the particle's passage through an electric field. Explicitly performing this integral for every collision would be very computationally expensive, given that the changes in  $\epsilon$  will depend on the velocity at which the particle is traveling and, for non-uniform electric fields, the position of the charged particle as well.

One popular approach uses the method of “null collisions” [14], where the collision frequency is calculated based on the maximum collision frequency  $\nu_0$  that the particle is likely to be able to reach during its transport. Using this constant collision frequency, equation (7) can be solved by equating  $P(\tau)$  with a uniformly distributed random number  $R$ , in which case

$$\tau = -\nu_0^{-1} \ln R. \quad (8)$$

When the collision occurs, a second random number is generated which is used to account for this overestimation by allowing the charged particle to undergo “null” collisions, where no exchange of energy or momentum occurs. This procedure suffers from a requirement to “backtrack” if the assumed collision frequency is too low, where it must then make a second assumption with a higher collision frequency. It is therefore important to minimize the number of null collisions and backtracks to optimize the simulation speed, and more modern simulations [24] have been designed with this in mind. The null collision method effectively amounts to a form of rejection method for sampling from  $P(\tau)$ , which means that potentially many random numbers are generated for each valid collision.

The simulation presented here uses an alternative approach. The cross-sections are specified as a function of energy, but are assumed to be constant within energy bins of width  $\delta\epsilon$ . These energy bins can be made arbitrarily small, so there is no loss of accuracy provided that we are careful to test that the results are independent of the bin width. However, this means that it is sufficient to recalculate  $\tau$  only when the energy of the particle changes from one bin to another, so until this occurs, the collision frequency in equation (8) remains constant. We therefore design the simulation so that particles can undergo two types of interactions. Collisions with neutral particles are described above, and are governed by  $i$ , the energy bin of the particle. The second type of interaction occurs when the energy bin is judged to have changed due to the effect of the electric field. In such an interaction, the only parameter that changes is  $i$ , which either increases or decreases by one, triggering a recalculation of the time until the next neutral particle interaction. The time until the change,  $t$ , is determined by analysis of the particle’s current velocity and the (constant) acceleration that it is experiencing due to the electric field. This is given by the smallest real, positive solution to the following equation for the kinetic energy:

$$\frac{1}{2}m(\mathbf{v}_0 + (\mathbf{a}t))^2 = \epsilon_i \pm \frac{1}{2}\delta\epsilon. \quad (9)$$

Recalculating the time until collision  $\tau$  does not require the use of another random number. Recalling equation (8), we now have additional terms for each change in energy bin:

$$\begin{aligned} \tau = t_0 + t_1 + \dots + t_n \\ -\nu_n^{-1} [\ln(R) - \nu_0 t_0 - \nu_1 t_1 - \dots - \nu_{n-1} t_{n-1}], \end{aligned} \quad (10)$$

where each  $t_i$  is determined by the time required for the particle to change energy from

one bin to the next, and each  $\nu_i$  represents the corresponding collision frequency for each energy bin at that time. This equation reduces to equation (8) in the case of constant  $\nu_n$  or zero  $t_i$ . In practice, the simulation maintains a running measure of the remaining ‘‘collision probability’’ for each particle. This is the dimensionless quantity in square brackets in equation 10 that is divided by the current  $\nu$  to calculate the time until next collision.

### III. BENCHMARK SYSTEM FOR MODELING COHERENT SCATTERING

#### A. Percus-Yevick Hard Sphere Model

To demonstrate and benchmark the new simulation procedure and code, we apply it to a simple model system that requires a correct treatment of structured media. One such model, frequently used in the literature, is that of a structure for hard-sphere potentials obtained by applying the Percus-Yevick approximation as a closure to the Ornstein-Zernike equation, which yields a pair-correlation function [25, 26], which in turn can be transformed into a static structure factor via a Fourier transform and directly used in our simulation. We use the Verlet and Weiss [18] structure factor, which includes some corrections to better emulate the structure of a real liquid:

$$S(\Delta k) = \left( 1 + \frac{24\eta}{\Delta k^2} \left[ \frac{2}{\Delta k^2} \frac{12\zeta}{\Delta k^2 - \beta} + \frac{\sin(\Delta k)}{\Delta k} \left( \alpha + 2\beta + 4\zeta - \frac{24\zeta}{\Delta k^2} \right) + \frac{2 \cos(\Delta k)}{\Delta k^2} \left( \beta + 6\zeta - \frac{12\zeta}{\Delta k^2} \right) - \alpha - \beta - \zeta \right] \right)^{-1}, \quad (11)$$

where  $\eta = \phi - \frac{\phi^2}{16}$ ,  $\alpha = \frac{(1+2\eta)^2}{(1-\eta)^4}$ ,  $\beta = \frac{-6\eta(1+\frac{\eta}{2})^2}{(1-\eta)^4}$  and  $\zeta = \frac{\eta\alpha}{2}$ . This includes a packing density parameter,  $\phi$ , which specifies how closely the hard spheres are packed. It can be written in terms of the hard sphere radius  $r$  and the neutral number density  $n_0$  as  $\phi = \frac{4}{3}\pi r^3 n_0$ . This structure factor depends only on the magnitude of the momentum exchange during a collision.

We have modeled systems with a range of densities, from  $\phi \approx 0$ , which approximates a dilute gas, to  $\phi = 0.4$ , which states that 40% of the volume is excluded by the hard-sphere potentials of the neutral molecules. The angle-integrated forms of each of these structure

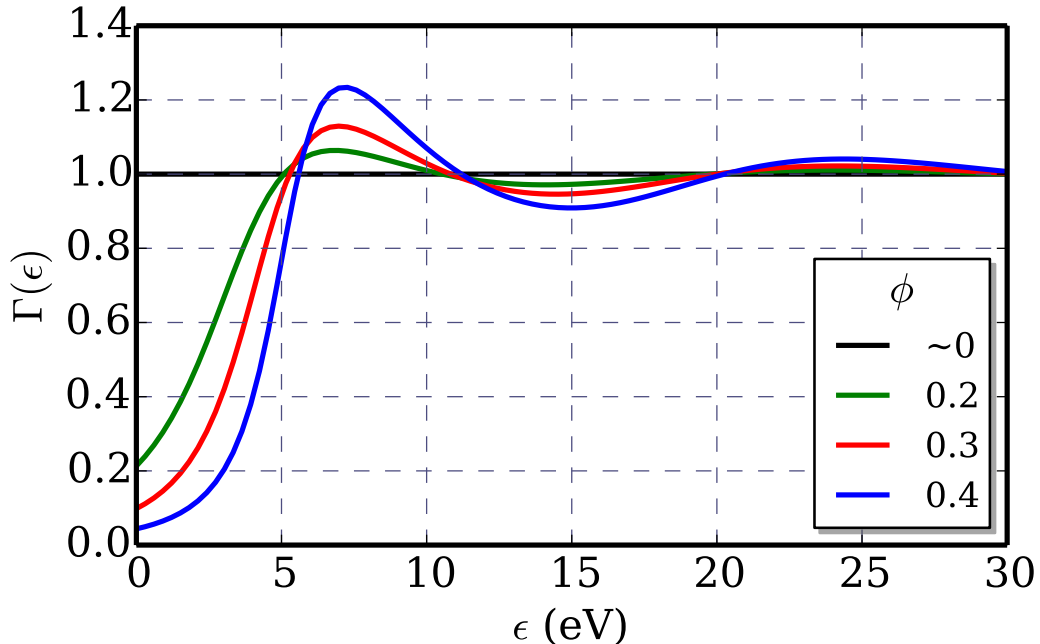


Figure 3. Angle integrated Percus-Yevick structure factors, from equations (11) and (5), as a function of particle energy and volume fraction.

factors, as described in equation (5), are shown in Fig. 3.

### B. System parameters

Our Monte Carlo codes use an event-by-event model, where every collision is considered independently. This allows for a great deal of flexibility in the specification of scattering mechanics, without any of the approximations used by “condensed history” simulations (see e.g. [27]). In addition, the swarm approximation — that all transport particles are independent — allows the simulation to be run in parallel. This makes it ideal for scheduled multi-processor batch jobs, where execution is not necessarily simultaneous or even sequential.

We have calculated a number of transport coefficients for comparison with other models. The meaning and derivation of all of these coefficients are described in [8] and [28], but a short summary is given here. All coefficients are measured as a discrete function of time-step  $t_i$ . During simulation, if a particle’s history crosses a time-step, its properties (eg:

position, velocity, position squared) at that time are sampled. We choose the z-axis to be aligned with the electric field, since it is the only element of the system that has a preferred direction. Each property is added to a separate running total for each time step, and after the simulation is complete, the totals are divided by the (in general) time-dependent total of the number of particles. This results in the average of a property over all particles, as a function of time. While the transport coefficients are in general time-varying, for the systems considered in this study all transport coefficients eventually reach a hydrodynamic equilibrium after sufficient time has passed. Afterwards, they merely fluctuate in a small statistical range about the reported equilibrium value.

Depending on the required transport coefficients, different properties of the charged particles must be recorded. In the following table, each definition [28] is of the named property at one point in time:

Transport coefficient	Definition
Mean energy	$\bar{\epsilon} = \langle \epsilon \rangle$
Bulk drift velocity	$W = \frac{d}{dt} \langle r_z \rangle$
Bulk longitudinal diffusion	$D_L = \frac{d}{dt} (\langle r_z^2 \rangle - \langle r_z \rangle^2)$
Bulk transverse diffusion	$D_T = \frac{1}{2} \sum_{i=x,y} \frac{d}{dt} (\langle r_i^2 \rangle - \langle r_i \rangle^2)$

Angle brackets denote an average over all particles,  $r_i$  represents the appropriate Cartesian coordinate of the position of the particle and  $\epsilon$  represents the energy of the particle.

In principle, there are two types of transport coefficients, known as “flux” and “bulk”, which approximately correspond to per-particle averages and system averages respectively [28]. However, because our model contains no non-conservative collision processes, the “flux” and “bulk” quantities should be identical, provided enough time samples are taken. We have chosen to measure “bulk” quantities where possible, because this implicitly averages over changes in velocity between time steps, whereas measuring the flux drift velocity and diffusion requires sampling instantaneous values at discrete time values. For the same number of time-steps, without any explicit time-averaging of velocity, the bulk quantities have far less statistical error.

Two ranges of reduced field strengths were used. An approximately logarithmic spacing of electric field strengths from 0.001 to 100 Td provides a broad picture of the resulting behaviors, while a linear spacing of field strengths from 2 to 12 Td provides detail in the range in which we expect the two Monte Carlo methods to disagree most strongly.

We employ the cold-gas limit, in which the neutrals are considered to be at rest. The present method does not accurately support non-zero neutral temperatures, as the static structure factor does not contain information about the temperature of the system. We are presently formulating a rigorous treatment of non-zero neutral temperatures using the dynamic structure factor [29].

All of our simulations were performed at different neutral densities as prescribed by the volume fraction  $\phi$  and the hard-sphere radius of the single particle cross section  $\sigma_{sp}$ . The transport properties presented are independent of the neutral number density, as it scales inversely with the electric field strength. In all cases, the hard-sphere cross section for single-particle scattering was set as  $\sigma_{sp}(\epsilon) = 6 \text{ \AA}^2$ , while the charged particles were assigned a mass equal to that of an electron,  $m = m_e$  and the mass of the neutrals was set to  $m_0 = 4 u$ .

## IV. RESULTS AND DISCUSSION

### A. Transport coefficients calculated with the new Monte Carlo method.

The Percus-Yevick hard-sphere system has been previously studied in [8], and a comparison with those results provides a test of our simulation [30]. Figure 4 shows the various transport coefficients simulated by the SSMC simulations, using the approach which overcomes Wojcik and Tachiya's approximation. It is instructive to compare this figure with Fig. 3, to see the field strengths that are affected most strongly by the features of the structure factors employed. A table of some of our results is in Appendix B, where we have compared them with Boltzmann equation results. The full dataset is available as supplementary material. We have simulated enough particles that in general the Monte Carlo statistical error [31] is not visible at these scales, being less than 1% in all cases. Agreement with the Boltzmann equation results is to within 1% in all cases, so the datasets would not be seen as distinct if shown in the above figures, but a detailed comparison is presented in section IV B.

The features of the results are discussed in detail in [8], and we will not repeat that discussion in depth here. One key feature is the presence of structure-induced negative-differential conductivity (defined in [32]) apparent in the drift velocity: at moderate field strengths of 1-10 Td, the drift velocity is inversely proportional to the field strength. This

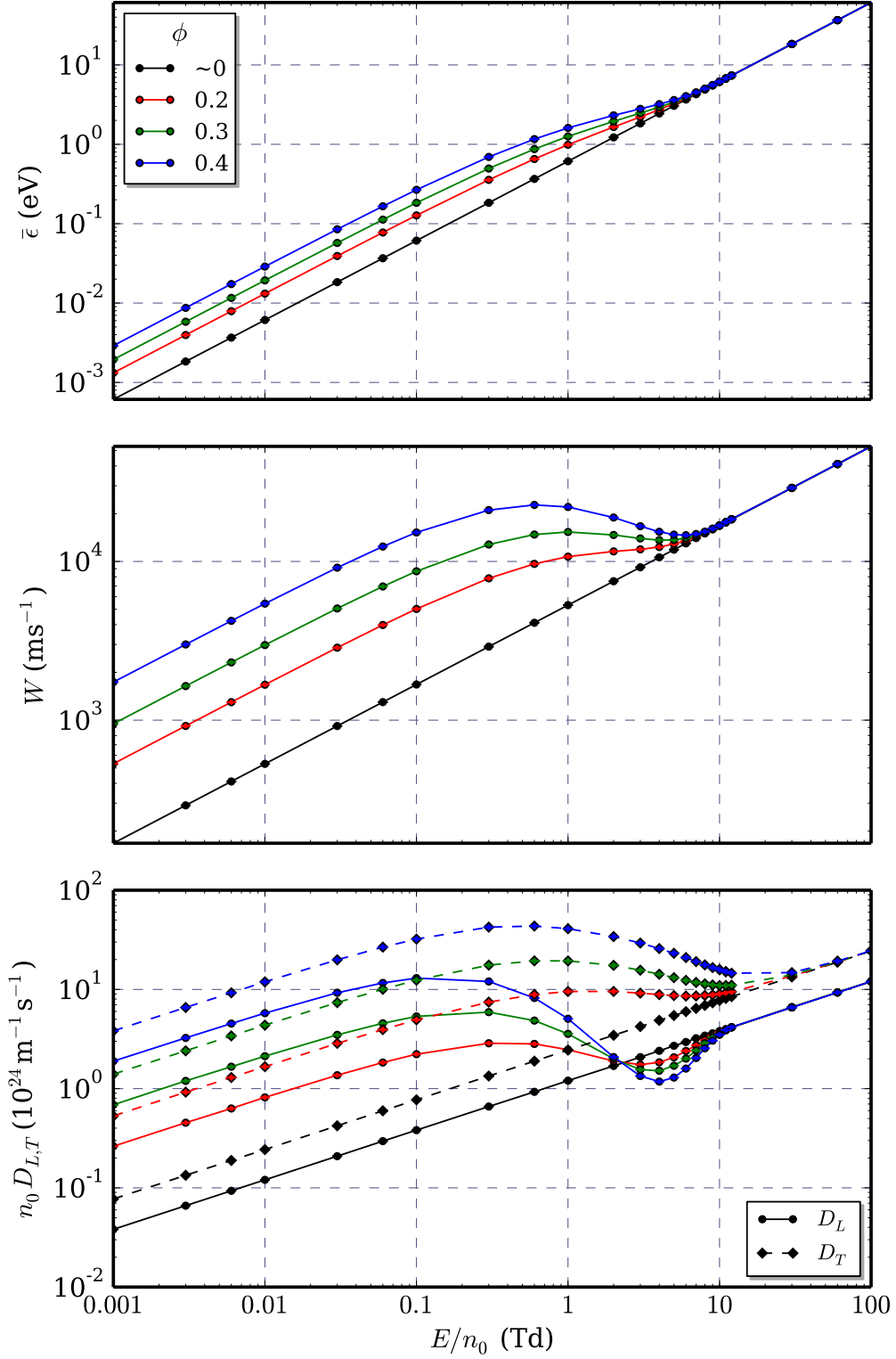


Figure 4. Mean energy  $\epsilon$ , drift velocity  $W$ , and diffusion coefficients  $D_L$  and  $D_T$  for Percus-Yevick model simulations, as a function of reduced electric field  $E/n_0$  and Percus-Yevick packing ratio  $\phi$ . Error bars are not visible at this scale.

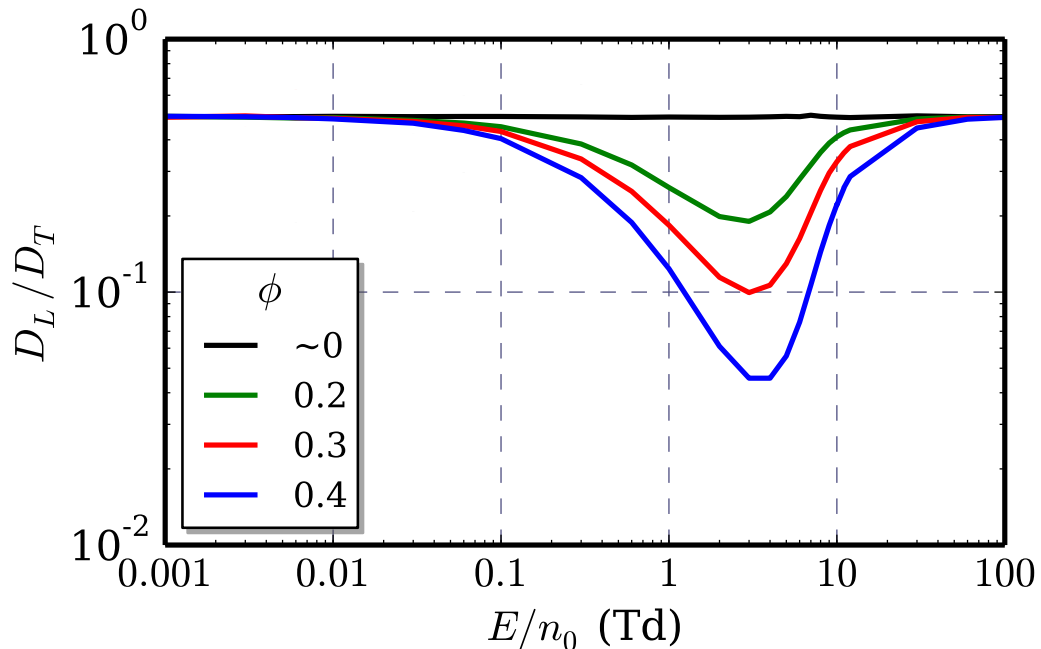


Figure 5. Ratio of diffusion coefficients as a function of reduced electric field strength  $E/n_0$  and packing ratio  $\phi$ . Note that the ratio for  $\phi \sim 0$  is 0.5 as required.

is because at low field strengths, the presence of coherent scattering causes an anisotropy in particle scattering which allows the particles to be affected more consistently by the field, raising their velocity in comparison to the structure-free case. At higher field strengths, the mean particle energy is higher, leading to a reduced de Broglie wavelength, which means that the charged particles interact with fewer neutral molecules, so the coherent effects are reduced. This results in a net reduction of forward motion despite a higher average energy.

We would also like to highlight the variation in the anisotropic diffusion as a function of  $\phi$ . In the case of a hard-sphere gas with no structure, we expect the ratio  $D_L/D_T = 0.5$  [7], which, as shown in Fig. 5, is demonstrated by our simulations. When structure is introduced, this ratio changes significantly. This effect has been previously explored in [8] and [21] through the extended Generalized Einstein Relation. We note that a multiterm Boltzmann equation solution is required to achieve the accuracy of the SSMC technique. The SSMC simulations have no difficulties in accurately representing this anisotropy in the velocity distribution function.

## B. Comparisons with Boltzmann equation and Wojcik and Tachiya's method.

In Fig. 6, we present the percentage difference between our SSMC and WT results and the Boltzmann equation solution. Our implementation of the WT method shows good agreement over most regions of field strength, however for some larger field strengths, errors of up to 5% in the mean energy and up to 35% in the diffusion coefficients become apparent. These differences occur when the energies of the electrons are within the regions that are truncated by the WT method. We can identify two competing factors that have an effect when the particle's energy is in these regions, causing differences between the SSMC and WT methods. Firstly, the collision frequency is enhanced, and since every collision has a chance of both removing some energy from the particle and changing the direction of the particle away from the direction of the electric field, this means that particles will tend to lose energy at a greater rate. However, this is balanced by the presence of the new momentum-only collision, which can occur up to 28% of the time in these regions. The presence of such collisions will tend to decrease the energy transfer rate. Nevertheless, Fig. 6 clearly shows that the combination of the effects is observable for the Percus-Yevick  $\phi = 0.4$  case, with a peak difference at approximately 8 Td. This corresponds to a mean energy of about 5 eV (see Fig. 4), which is at the peak of the  $\Gamma(\epsilon)$  function. That peak is where we would expect the WT approximation to be least suitable.

For the present model, the disagreements with the Boltzmann equation results are less than 1% over all field strengths considered. Such differences are of the order of the numerical schemes used in the SSMC and Boltzmann equation methods. We suspect the remaining differences are a result of energy meshes used in the Monte Carlo codes or Boltzmann equation numerical solutions.

## V. CONCLUDING REMARKS

We have presented a new Monte Carlo simulation code which accurately accounts for the effects of structure in non-gaseous systems by employing a modified mechanistic per-collision interpretation of the Cohen and Lekner method for solving the Boltzmann equation. The SSMC results accurately replicate those calculated via a multi-term solution of the Boltzmann equation to within 1%, with agreement significantly improved over those results

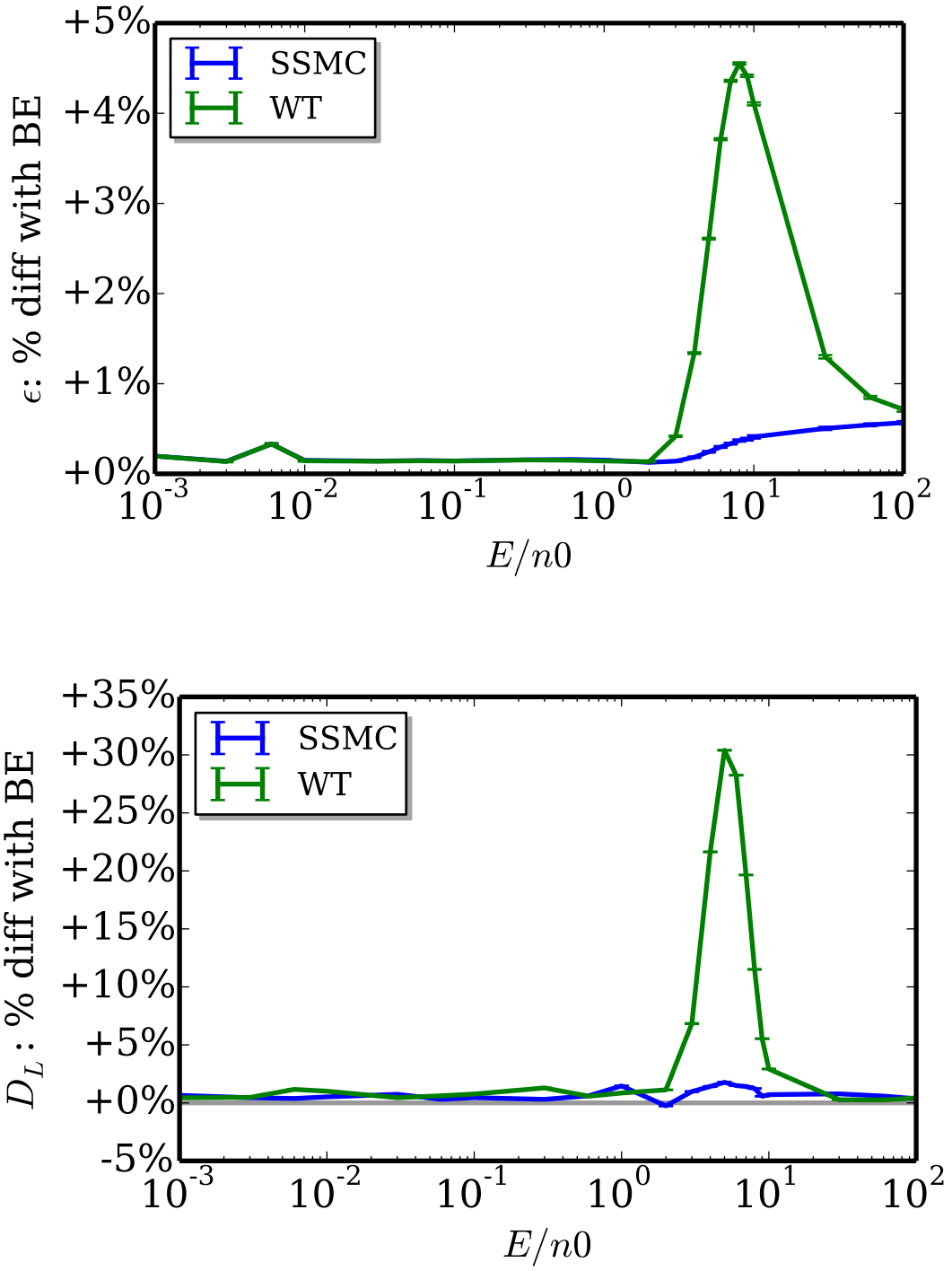


Figure 6. Mean energy  $\epsilon$  and longitudinal diffusion  $D_L$  percentage difference for each Monte Carlo model versus the Boltzmann equation (BE) model, for the Percus-Yevick structure factor at  $\phi = 0.4$ .

obtained using the WT method, where errors of up to 35% were observed in some transport coefficients. Future work will be focused on utilizing a dynamic structure factor to account for other structural and collective effects, including non-zero background temperatures.

- 
- [1] M. Wojcik and M. Tachiya, *Chemical Physics Letters* **363**, 381 (2002).
- [2] D. Carlson and C. Wronski, *Amorphous Semiconductors*, 2nd ed., edited by M. H. Brodsky (Springer Berlin Heidelberg, 1985) pp. 113–158.
- [3] H. Nikjoo, M. Terrissol, R. Hamm, J. Turner, S. Uehara, H. Paretzke, and D. Goodhead, *Radiation Protection Dosimetry* **52**, 165 (1994).
- [4] D. W. Gidley, H.-G. Peng, and R. S. Vallery, *Annual Review of Materials Research* **36**, 49 (2006).
- [5] I. Buvat, I. Castiglioni, J. Feuardent, and M. C. Gilardi, *Physics in Medicine and Biology* **50**, 329 (2005).
- [6] I. Kawrakow and A. Bielajew, *Nuclear Instruments and Methods in Physics Research B* **142**, 253 (1998).
- [7] R. E. Robson, *Introductory Transport Theory for Charged Particles in Gases* (World Scientific, Singapore, 2006).
- [8] R. D. White and R. E. Robson, *Physical Review E* **84**, 1 (2011).
- [9] A. O. Allen, P. J. Kuntz, and W. F. Schmidt, *The Journal of Physical Chemistry* **88**, 3718 (1984).
- [10] C. Champion, C. Le Loirec, and B. Stosic, *International journal of radiation biology* **88**, 54 (2012).
- [11] D. Emfietzoglou, K. Karava, G. Papamichael, and M. Moscovitch, *Physics in Medicine and Biology* **48**, 2355 (2003).
- [12] M. Šuvakov, Z. L. Petrović, J. P. Marler, S. J. Buckman, R. E. Robson, and G. Malović, *New Journal of Physics* **10**, 053034 (2008).
- [13] A. Muñoz, J. M. Pérez, G. García, and F. Blanco, *Nuclear Instruments and Methods in Physics Research Section A: Accelerators, Spectrometers, Detectors and Associated Equipment* **536**, 176 (2005).
- [14] H. R. Skullerud, *Journal of Physics D: Applied Physics* **1**, 1567 (1968).
- [15] Y. Sakai, K. Sukegawa, S. Nakamura, and H. Tagashira, *IEEE Transactions on Electrical Insulation* **23**, 609 (1988).
- [16] C. Champion and C. Le Loirec, *Physics in medicine and biology* **51**, 1707 (2006).

- [17] P. Verkerk, U. Bafle, F. Barocchi, L. de Graaf, J.-B. Suck, and H. Mutka, *Physical Review Letters* **67**, 1262 (1991).
- [18] L. Verlet and J.-J. Weis, *Physical Review A* **5**, 939 (1972).
- [19] M. Cohen and J. Lekner, *Physical Review* **158**, 305 (1967).
- [20] L. Van Hove, *Physical Review* **95**, 249 (1954).
- [21] G. J. Boyle, R. D. White, R. E. Robson, S. Dujko, and Z. L. Petrovic, *New Journal of Physics* **14** (2012), 10.1088/1367-2630/14/4/045011.
- [22] Note that single-particle cross sections are ideally defined in terms of the collision energy, which depends on the relative speed of the particle in the center of mass frame of the collision. However, in practice, most measured cross sections are, by necessity, the integral of the cross section of all possible relative speeds, weighted by their frequency according to the neutral particle's velocity distribution. The differences are very small for electrons impacting on even the lightest atoms, although they may be significant for ion scattering at very low energies.
- [23] M. J. Brennan, A. M. Garvie, and L. J. Kelly, *Australian Journal of Physics* **43**, 27 (1990).
- [24] M. J. Brennan, *IEEE Transactions on Plasma Science* **19**, 256 (1991).
- [25] M. Wertheim, *Physical Review Letters* **10** (1963).
- [26] E. Thiele, *The Journal of Chemical Physics* **39**, 474 (1963).
- [27] A. E. Nahum, *Radiation and Environmental Biophysics* **38**, 163 (1999).
- [28] S. Dujko, R. D. White, and Z. L. Petrović, *Journal of Physics D: Applied Physics* **41**, 245205 (2008).
- [29] W. J. Tattersall, D. G. Cocks, and R. D. White, Manuscript in preparation (2015).
- [30] An error in the calculation of the Percus-Yevick structure factor used in [8] means that the structure factor would be correct for a fluid where the molecules have a hard-sphere cross-section of  $\sigma = 1.5 \text{ \AA}^2$ , not the reported cross-section of  $\sigma = 6 \text{ \AA}^2$ , although the cross-sections themselves were as reported. The Boltzmann equation results presented here have been recalculated with the correct structure factor, as described in section III A. The phenomenology reported in [8] remains correct, however.
- [31] E. Koehler, *The American Statistician* **63**, 155 (2009).
- [32] R. White and R. Robson, *Physical Review Letters* **102**, 1 (2009).

## Appendix A: Comparison between Monte-Carlo and Boltzmann equation averages

As discussed in section II B, the three different processes in the SSMC have been chosen in order to reproduce the mean rate of transfer of energy and momentum that was obtained in the derivation of the Boltzmann equation. These different processes, corresponding to the “cross sections” defined in the main text, are:  $\sigma_{\text{both}}$ , a normal collision that exchanges both energy and momentum;  $\sigma_{\text{energy}}$ , a collision without direction change that aims to allow only energy exchange; and  $\sigma_{\text{momentum}}$ , a collision with only momentum exchange. In this appendix we show that, for isotropic scattering from stationary neutrals (i.e. we consider only  $T = 0$  as in accordance with the regime of validity of the Monte-Carlo simulations), these processes give rise to the same rates of energy and momentum transfer as the Boltzmann equation, after neglecting terms dependent on the mass-ratio  $m/m_0$ . Note that in this appendix, dashes refer to post-collision quantities.

In a collision, it is appropriate to consider the particle in the center of mass frame. In this frame, isotropic scattering implies that the particle’s relative velocity  $\mathbf{v}_{\text{rel}} = \mathbf{v} - \mathbf{g}$ , where  $\mathbf{g}$  is the velocity in the center of mass frame, is unchanged in magnitude ( $|v'_{\text{rel}}| = |v_{\text{rel}}|$ ) and with a randomly assigned angle such that all values of  $\cos \chi$ , where  $\chi$  is the scattering angle, are equally likely. We assume, without loss of generality, that the direction of the particle’s velocity prior to the collision is aligned with the  $z$  axis. Note that we do not need to consider the electric field in this discussion.

For a normal (“both”) collision, one can easily show [7] that scattering from a stationary neutral leads to an angle-dependent energy change given by

$$\Delta\epsilon_{\text{both}} = \epsilon \frac{2mm_0}{(m + m_0)^2} (\cos \chi - 1), \quad (\text{A1})$$

and a change of the  $z$ -component of the momentum given by

$$\Delta v_{z,\text{both}} = \frac{m_0}{m + m_0} v (\cos \chi - 1). \quad (\text{A2})$$

Hence the average transfer of energy is

$$\langle \Delta\epsilon \rangle_{\text{both}} = \frac{1}{2} \int_{-1}^1 \Delta\epsilon_{\text{both}} d \cos \chi \quad (\text{A3})$$

$$= 2mm_0\epsilon / (m + m_0)^2 \quad (\text{A4})$$

and the average transfer of momentum, for which the components perpendicular to  $z$  average

to zero, is

$$\langle \Delta v_z \rangle_{\text{both}} = -m_0 v_z / (m + m_0). \quad (\text{A5})$$

For an “energy-only” collision, we select a random change in energy through a random “false” angle  $\chi$ , and calculate the energy change as if a normal collision through this angle had occurred. This preserves the average transfer of energy  $\langle \Delta \epsilon \rangle_{\text{energy}} = \langle \Delta \epsilon \rangle_{\text{both}}$ . We then discard the angle  $\chi$ , resetting the direction of motion of the particle to that before the collision. This has the unfortunate side effect of producing a change in momentum, contrary to the purpose of producing a collision with no momentum transfer. The change of momentum in this case is simply given by:

$$\begin{aligned} \Delta v_{z,\text{energy}} &= \sqrt{\frac{2}{m}} \left( \sqrt{\epsilon - \Delta \epsilon(\chi)} - \sqrt{\epsilon} \right) \\ &= v \left( \sqrt{1 + \frac{2mm_0}{(m+m_0)^2} (\cos \chi - 1)} - 1 \right) \end{aligned} \quad (\text{A6})$$

and upon averaging over  $\cos \chi$  we find:

$$\begin{aligned} \langle \Delta v_z \rangle_{\text{energy}} &= -v \left[ 1 - \frac{1}{3a} (1 - (1 - 2a)^{3/2}) \right] \\ &= -\frac{m(3m_0 - m)v_z}{3m_0(m + m_0)} \end{aligned}$$

where  $a = 2mm_0/(m + m_0)^2$ , and the second result is arrived at after some algebraic manipulations, under the assumption that  $m < m_0$ .

For a “momentum only” collision, we perform a collision as normal using an angle  $\chi$  but set the post-collision energy to the pre-collision energy. Hence, it is obvious that  $\langle \Delta \epsilon \rangle_{\text{momentum}} = 0$  but the modification of the energy also has an impact on the average momentum change, which we calculate below. Note that  $\mathbf{v}' = v\hat{\mathbf{v}}'$ , where  $\hat{\mathbf{v}}'$  is identical to that of a normal collision. Hence,

$$\mathbf{v}'_{\text{both}} \cdot \hat{\mathbf{z}} = \frac{v}{m + m_0} (m_0 \cos \chi + m) \quad (\text{A7})$$

implies that

$$\begin{aligned} \hat{\mathbf{v}}' \cdot \hat{\mathbf{z}} &= \frac{\mathbf{v}'_{\text{both}} \cdot \hat{\mathbf{z}}}{|\mathbf{v}'_{\text{both}}|} \\ &= \frac{\cos \chi + \frac{m}{m_0}}{\sqrt{1 + 2\frac{m}{m_0} \cos \chi + \frac{m^2}{m_0^2}}} \end{aligned} \quad (\text{A8})$$

From this, we find the change in the  $z$ -component of momentum of a single collision

$$\Delta v_{z,\text{momentum}} = (\mathbf{v}' - \mathbf{v}) \cdot \hat{\mathbf{z}} = v(\hat{\mathbf{v}}' \cdot \hat{\mathbf{z}} - 1) \quad (\text{A9})$$

and hence obtain an average momentum transfer of

$$\begin{aligned} \langle \Delta v_z \rangle_{\text{momentum}} &= \frac{v}{2} \int_{-1}^1 \left( \frac{\cos \chi + \frac{m}{m_0}}{\sqrt{1 + 2\frac{m}{m_0} \cos \chi + \frac{m^2}{m_0^2}}} - 1 \right) d \cos \chi \\ &= -v_z \left( 1 - \frac{2}{3} \frac{m}{m_0} \right) \end{aligned} \quad (\text{A10})$$

We must now combine these averages. In the Monte-Carlo simulation there are two distinct regimes depending on the value of  $\Gamma(\epsilon)$ . If  $\Gamma(\epsilon) < 1$ , then the  $\sigma_{\text{both}}$  and  $\sigma_{\text{energy}}$  cross sections occur with frequencies such that:

$$\begin{aligned} \left. \frac{d\langle \epsilon \rangle}{dt} \right|_{\Gamma(\epsilon) < 1} &= \nu_{\text{sp}} \Gamma(\epsilon) \langle \Delta \epsilon \rangle_{\text{both}} + \nu_{\text{sp}} (1 - \Gamma(\epsilon)) \langle \Delta \epsilon \rangle_{\text{energy}} \\ &= \nu_{\text{sp}} \langle \Delta \epsilon \rangle_{\text{both}} \\ &= \nu_{\text{sp}} \frac{2mm_0}{(m + m_0)^2} \epsilon \end{aligned} \quad (\text{A11})$$

where  $\nu_{\text{sp}}(v) = n_0 v \sigma_{\text{sp}}(v)$  would be the collision frequency in the absence of structure effects, and

$$\begin{aligned} m \left. \frac{d\langle \mathbf{v} \rangle}{dt} \right|_{\Gamma(\epsilon) < 1} &= m \nu_{\text{sp}} \Gamma(\epsilon) \langle \Delta \mathbf{v} \rangle_{\text{both}} + m \nu_{\text{sp}} (1 - \Gamma(\epsilon)) \langle \Delta \mathbf{v} \rangle_{\text{energy}} \\ &\approx -\frac{mm_0 \nu_{\text{sp}} \mathbf{v}}{m + m_0} \Gamma(\epsilon) + O\left(\frac{m}{m_0}\right), \end{aligned} \quad (\text{A12})$$

where we have generalized the momentum transfer for any initial velocity direction, i.e. by replacing  $v_z$  in equations (A5) and (A10) by  $\mathbf{v}$ . In order to compare to the Boltzmann equations, we first note that  $\sigma_m(v) = \sigma_{\text{sp}}(v)$  for isotropic scattering and hence  $\nu_{\text{sp}} = v\Lambda_0^{-1}$  and  $\nu_{\text{sp}}\Gamma(\epsilon) = v\Lambda_1^{-1}$ . Hence, we can see that these rates of transfer are in agreement with the results for the Boltzmann equation (3) and (4), excepting some factors of order  $m/m_0$  that are neglected in our simulations and in the derivation of the Boltzmann equation. If  $\Gamma(\epsilon) > 1$  then the “both” and “momentum only” cross sections occur with frequencies such

that:

$$\begin{aligned}
\left. \frac{d\langle\epsilon\rangle}{dt} \right|_{\Gamma(\epsilon)>1} &= \nu_{\text{sp}}\langle\Delta\epsilon\rangle_{\text{both}} + \nu_{\text{sp}}(\Gamma(\epsilon) - 1)\langle\Delta\epsilon\rangle_{\text{momentum}} \\
&= \nu_{\text{sp}}\frac{2mm_0}{(m + m_0)^2}\epsilon
\end{aligned} \tag{A13}$$

and

$$\begin{aligned}
m \left. \frac{d\langle\mathbf{v}\rangle}{dt} \right|_{\Gamma(\epsilon)>1} &= m\nu_{\text{sp}}\langle\Delta v\rangle_{\text{both}} + m\nu_{\text{sp}}(\Gamma(\epsilon) - 1)\langle\Delta v\rangle_{\text{momentum}} \\
&\approx -\frac{mm_0\nu_{\text{sp}}\mathbf{v}}{m + m_0}\Gamma(\epsilon) + O\left(\frac{m}{m_0}\right)
\end{aligned} \tag{A14}$$

and again we recover the Boltzmann equation results with negligible factors of  $m/m_0$ .

We note that it is possible to correct for these differences of the order of  $m/m_0$  by modifying the cross sections  $\sigma_{\text{energy}}$  and  $\sigma_{\text{momentum}}$ . However, this would only be necessary if we considered systems in which the mass ratios were close to unity.

Finally, we comment on the difference between the SSMC and WT methods. Wojcik and Tachiya [1] had mentioned that, in their particular calculation, they assumed the structure factor was mostly smaller than unity, which also implies that  $\Gamma(\epsilon) < 1$ . They did not deal with values greater than unity, instead choosing to set  $\Gamma(\epsilon) = \min(\Gamma(\epsilon), 1)$ . This means that the rates of energy and momentum transfer are unchanged when  $\Gamma(\epsilon) < 1$  and continue to follow equations (A11) and (A12). However, for  $\Gamma(\epsilon) > 1$ , this leads to an error in the WT method in the momentum transfer which is of the order:

$$-\frac{mm_0\nu_{\text{sp}}v}{m + m_0}(\Gamma(\epsilon) - 1). \tag{A15}$$

There is no error in the energy transfer using the WT method.

## Appendix B: Benchmark Values for Transport Coefficients

$\phi$	$E/n_0$ (Td)	Mean energy (eV)			Drift Velocity ( $\text{ms}^{-1}$ )		
		BE	SSMC	Diff.	BE	SSMC	Diff.
0.0	0.03	0.018232	$0.018338 \pm 0.023\%$	0.58%	910.63	$918.52 \pm 0.0058\%$	0.86%
	0.3	0.18232	$0.1834 \pm 0.022\%$	0.59%	2879.7	$2905.6 \pm 0.0064\%$	0.90%
	3	1.8232	$1.8333 \pm 0.02\%$	0.55%	9106.3	$9186.5 \pm 0.0074\%$	0.88%
	10	6.077	$6.113 \pm 0.022\%$	0.58%	16626	$16783 \pm 0.0096\%$	0.94%
	30	18.232	$18.34 \pm 0.024\%$	0.58%	28797	$29077 \pm 0.01\%$	0.97%
0.2	0.03	0.039039	$0.039149 \pm 0.012\%$	0.28%	2851.35	$2861.91 \pm 0.002\%$	0.37%
	0.3	0.35569	$0.35667 \pm 0.015\%$	0.27%	7797	$7827.7 \pm 0.0027\%$	0.39%
	3	2.2039	$2.2102 \pm 0.014\%$	0.28%	11860.7	$11921.1 \pm 0.0066\%$	0.50%
	10	6.112	$6.141 \pm 0.017\%$	0.48%	16726	$16851.5 \pm 0.0055\%$	0.75%
	30	18.25	$18.351 \pm 0.023\%$	0.55%	28833	$29071 \pm 0.0048\%$	0.82%
0.3	0.03	0.057118	$0.057228 \pm 0.01\%$	0.19%	5044.64	$5055.53 \pm 0.0011\%$	0.21%
	0.3	0.49489	$0.49585 \pm 0.01\%$	0.19%	12756.1	$12788.1 \pm 0.0016\%$	0.25%
	3	2.4654	$2.4703 \pm 0.012\%$	0.20%	13909	$13959.3 \pm 0.0047\%$	0.36%
	10	6.127	$6.152 \pm 0.017\%$	0.41%	16756.5	$16863.1 \pm 0.004\%$	0.63%
	30	18.259	$18.354 \pm 0.015\%$	0.51%	28852.2	$29065.3 \pm 0.0031\%$	0.73%
0.4	0.03	0.084858	$0.084979 \pm 0.0098\%$	0.14%	9132.66	$9139.8 \pm 0.00079\%$	0.08%
	0.3	0.69229	$0.69337 \pm 0.0083\%$	0.15%	21031.8	$21066.9 \pm 0.0012\%$	0.16%
	3	2.7924	$2.7963 \pm 0.0065\%$	0.14%	16637.7	$16680.3 \pm 0.0038\%$	0.25%
	10	6.14	$6.165 \pm 0.018\%$	0.40%	16767.6	$16871.6 \pm 0.0033\%$	0.62%
	30	18.269	$18.361 \pm 0.017\%$	0.50%	28872.5	$29076.6 \pm 0.0028\%$	0.70%

Table I. Benchmark values for transport coefficients: mean energy and drift velocity. Boltzmann equation (BE) results are compared with the SSMC results. Quoted error is twice the standard error in the mean of the SSMC results. Comparisons between BE and SSMC are shown as a third sub-column for each type of transport coefficient.

$\phi$	$E/n_0$ (Td)	$n_0 D_L$ ( $10^{24} \text{ m}^{-1} \text{ s}^{-1}$ )			$n_0 D_T$ ( $10^{24} \text{ m}^{-1} \text{ s}^{-1}$ )		
		BE	SSMC	Diff.	BE	SSMC	Diff.
0.0	0.03	0.20726	$0.20859 \pm 0.01\%$	0.64%	0.42195	$0.4224 \pm 0.0041\%$	0.10%
	0.3	0.65543	$0.66011 \pm 0.011\%$	0.71%	1.33432	$1.33984 \pm 0.006\%$	0.41%
	3	2.0726	$2.0767 \pm 0.014\%$	0.19%	4.2195	$4.2261 \pm 0.0059\%$	0.15%
	10	3.7841	$3.8073 \pm 0.012\%$	0.61%	7.7037	$7.7459 \pm 0.0067\%$	0.54%
	30	6.5543	$6.6398 \pm 0.012\%$	1.30%	13.3432	$13.3487 \pm 0.0059\%$	0.04%
0.2	0.03	1.35966	$1.36532 \pm 0.006\%$	0.41%	2.8418	$2.8603 \pm 0.0091\%$	0.65%
	0.3	2.8614	$2.8671 \pm 0.0092\%$	0.19%	7.4604	$7.4461 \pm 0.0032\%$	-0.19%
	3	1.7277	$1.7446 \pm 0.022\%$	0.97%	9.1902	$9.1665 \pm 0.0066\%$	-0.25%
	10	3.677	$3.7075 \pm 0.018\%$	0.82%	9.0054	$9.0232 \pm 0.0048\%$	0.19%
	30	6.5411	$6.5948 \pm 0.012\%$	0.82%	13.6167	$13.6324 \pm 0.0042\%$	0.11%
0.3	0.03	3.4743	$3.4834 \pm 0.0071\%$	0.26%	7.3668	$7.3715 \pm 0.0086\%$	0.06%
	0.3	5.8751	$5.9043 \pm 0.0076\%$	0.49%	17.561	$17.571 \pm 0.0048\%$	0.06%
	3	1.5321	$1.5553 \pm 0.018\%$	1.50%	15.651	$15.626 \pm 0.0074\%$	-0.15%
	10	3.5985	$3.5869 \pm 0.023\%$	-0.32%	11.029	$10.952 \pm 0.0096\%$	-0.70%
	30	6.5336	$6.5951 \pm 0.0065\%$	0.94%	13.985	$13.991 \pm 0.0072\%$	0.04%
0.4	0.03	9.182	$9.2498 \pm 0.0041\%$	0.73%	19.8166	$19.8841 \pm 0.004\%$	0.34%
	0.3	11.9922	$12.0287 \pm 0.0071\%$	0.30%	42.211	$42.43 \pm 0.0069\%$	0.51%
	3	1.3271	$1.34 \pm 0.027\%$	0.97%	29.2923	$29.3425 \pm 0.0017\%$	0.17%
	10	3.4836	$3.5084 \pm 0.0072\%$	0.71%	15.81	$15.813 \pm 0.0067\%$	0.02%
	30	6.526	$6.5769 \pm 0.0062\%$	0.77%	14.7608	$14.7684 \pm 0.0038\%$	0.05%

Table II. Benchmark values for transport coefficients: longitudinal and transverse diffusion, and energy gradient parameter. Boltzmann equation (BE) results are compared with the SSMC results. Quoted error is twice the standard error in the mean of the SSMC results. Comparisons between BE and SSMC are shown as a third sub-column for each type of transport coefficient.